UDK 661.183.2+628.16.094.3-926.214

Khaled Hosni, Ezzeddine Srasra

EVALUATION OF FLUORIDE REMOVAL FROM WATER BY HYDROTALCITE-LIKE COMPOUNDS SYNTHESIZED FROM THE KAOLINIC CLAY

The present study investigates the fluoride sorption by Mg – Al – CO_3 prepared from a kaolinite as natural source of aluminium using two simple methods. The first method uses the kaolinite in natural solid state; the second method uses the filtrate of the kaolinite after dissolution by acidic solutions. The adsorption characteristics of the fluoride from synthetic wastewater on calcined LDH samples were evaluated under laboratory conditions. The anionic clays tested were [K_{sd}3P10-T150] synthesized by method (1) using kaolinitic clay in solid state and [K_{liq}3P10] synthesized by method (2). The equilibrium isotherm showed that the uptake of fluoride ion was consistent with the Langmuir and Freundlich equations and that the Freundlich model gave a better fit to the experimental data than the Langmuir model. The maximum adsorption capacity is 238 and 175 mg/g for K_{liq}P10-(500)-LDH and K_{sd}P10-(500)-LDH, respectively, higher than that reported on other adsorbents for fluoride removal A mechanism for removal of fluoride ion has been confirmed by X-ray diffraction.Overall, the results demonstrate the convenient synthesis of the hydrotalcite from the kaolinite and the high efficiency of fluoride removal that is promising for potential applications of calcined K_{liq}P10 and K_{sd}P10-LDH in the environmental clean-up and remediation of contaminated water.

Keywords: adsorption; fluoride; hydrotalcite; kaolinite; layered compound; X-ray diffraction.

1. Introduction

Fluoride is an important micronutrient in human beings which, when consumed excessively, may lead to various diseases such as fluorosis, osteoporosis, arthritis, cancer, brain damage, Alzheimer syndrome and thyroid disorder [1]. The maximum acceptable concentration of fluoride in drinking water as regulated by World Health Organization is 1.5 mg/L [2]. Presence of fluoride in drinking water above acceptable concentration increased cases of fluorosis among the people has been reported from all over the world including China, India, Pakistan and Thailand [3].

Several defluoridation methods proposed and tested worldwide are mostly based on the principles of precipitation, ion exchange and adsorption. A wide variety of adsorbents have been tested for the abatement of fluoride from water. These include activated and impregnated alumina [4 – 8], cation exchanged

© KHALED HOSNI, EZZEDDINE SRASRA, 2011

zeolite F-9 [9], activated clay [10], carbonaceous materials [11 – 12], solid industrial wastes like red mud, fly ash and spent catalysts [13 – 14]. However, the defluoridation methods developed so far lack viability at the end-user level due to one or more reasons such as high cost technology, limited efficiency, unnoticeable break through, deteriorated water quality and taboo limitations [15].

Application of LDHs for defluoridation of water has attracted attention as LDHs are prepared in aqueous medium from low-cost precursors and can be easily regenerated. Layered double hydroxides (LDHs), also known as hydrotalcite-like compounds (HTlc) or anionic clays, consist of brucite-like hydroxide sheets, where partial substitution of trivalent for divalent cations results in a positive sheet charge compensated by anions within interlayer galleries [16]. Calcined $Mg - Al - CO_3$ form of LDHs have been demonstrated to reconstruct their original layered structure after the adsorption of various anions and are good ion exchangers/adsorbents for removal of toxic anions from contaminated water [17 – 21]. In the light of this so-called "memory effect" [22], the removal of fluoride from aqueous solution by calcined LDHs was studied. In this work, a detailed study on the synthesis of $Mg - Al - CO_3$ LDHs, by coprecipitaion and by mechanochemical synthesis method using kaolinite as aluminium source, their characterization and the influence of different parameters viz: initial fluoride concentration, time and solution pH on their performance in the adsorption of fluoride from water have been presented. The mechanism for removal of fluoride ion has been confirmed by X-ray diffraction (XRD).

2. Experimental

2.1. Material preparation. The $Mg - Al - CO_3$ hydrotalcite-like layered compounds has been synthesized by two methods using kaolinite as a natural source of trivalent cation and an aqueous solution of Na_2CO_3 as the precipitant**.**

Preparation of K_{sd}3P10. The sample was synthesized by crushing kaolinite with the magnesium nitrate hexahydrate (their amounts were so as to have the desired Mg^{2+}/Al^{3+} molar ratio), followed by heating at 500°C for 4 h. The product obtained was dispersed under constant stirring in an aqueous solution containing Na_2CO_3 (100 ml). The pH of the dispersion was maintained constant at 10 ± 0.1 by adding NaOH or HNO_3 when necessary. The slurry was subsequently agitated at room temperature for 24 h, and then aged at 150°C for 24 h. The resulting products were collected by centrifugal separation and washed thoroughly with deionised water to eliminate excess Na^+ followed by drying overnight at room temperature.

The samples were identified as [K_{sd}3P10-150], where K_{sd} represents the trivalent cation source (kaolinite) used to prepare the materials and "sd" represents the solid state. For example, K_{sd}3P10-T150 stands for the product prepared with kaolinite in solid state, an Mg/Al ratio of 3, an aging temperature of 150°C, and a pH of synthesis of 10.

Preparation of K_{liq}3P10. The sample was synthesized using as aqueous solution of Na_2CO_3 as precipitant. The solutions containing $Mg(NO_3)_2.6H_2O$ and Al^{3+}, cation resulting from dissolution of the purified kaolinite by acidic attack, (their concentration varied so as to have the Mg/Al molar ratio of 3) were added dropwise to the aqueous solutions of Na_2CO_3 with vigorous stirring. The pH of the dispersion was maintained constant at 10 ± 0.1 by adding NaOH (10%). The slurry was subsequently agitated at room temperature for three day. The resulting products were collected by centrifugal separation and washed thoroughly with deionised water to eliminate excess Na^+ followed by drying overnight at room temperature. The samples were identified as [K_{liq}3P10], where K_{liq} represents the trivalent cation source (kaolinite) used to prepare the materials and "liq" represents its liquid state. For example, K_{liq}3P10 stands for the product prepared with kaolinite in liquid state, an Mg/Al ratio of 3 and a pH of synthesis of 10.

2.2. Characterization of materials. The dried precipitates were characterized by XRD in order to determine the species present and their degree of crystallinity. Diffractograms were obtained by using a 'PANalytical X'Pert HighScore Plus' diffractometer using monochromated CuKα radiation. Nitrogen adsorption measurements were performed at -196°C with an Autosorb-1 unit (Quantachrome, USA) for the determination of sample textural properties using the multipoint Brunaner-Emmet-Teller (BET) method. The samples were out gassed at 120°C under a vacuum at 10^{-3} mm Hg for 3.5 h. Fourier-transformed infrared (FT-IR) spectra were recorded as KBr pellets using a Perkin-Elmer FT-IR (model 783) instrument. KBr pellets were prepared by mixing 5 wt % anionic clay with 95 wt % KBr and pressing.

2.3. Fluoride sorption experiments. The samples used in the sorption experiments were identified as K_{sd}3P10-(500) and K_{liq}3P10-(500). These two adsorbents were obtained by the heating of K_{sd}3P10 and K_{liq}3P10 in a muffle furnace at 500°C for 4 h. All solutions were prepared and stocked in polyethylene flasks. The adsorption experiments were carried out in 50 ml polyethylene tubes. Fluoride stock solutions were prepared from NaF. Most of the experiments were carried out at the room temperature (around 25 °C). Analysis of F concentrations in the samples was done using F ion selective electrode (FISE) Model 9609BN [23]. FISE was calibrated using standard F solutions in the concentration range 5 – 50 mg/L — a range in which the electrode exhibited true Nernstian response. The results were plotted as fluoride concentration (mg/L) versus potential (mV). The observed selectivity ratio of the electrode was $< 10^{-3}$ for all the ions, except OH^-. For F estimation, 10 ml aliquots were mixed with 10 ml of total ionic strength adjusting buffer (TISAB). This buffer contains a chelate, which forms complexes with other ions, such as iron and aluminum that could interfere in the determination. Each litre of TISAB contained 58 g NaCl, 57 ml glacial acetic acid, 0.3 g tri-sodium citrate and sufficient NaOH to yield a pH of 5.3.

The time-dependent sorption of fluoride on calcined K_{sd}3P10-LDH and K_{liq}3P10-LDH was carried out with 100 mg of the adsorbent and 20 ml of

1000 mg·L^{-1} of fluoride solution. The mixture was stirred at low speed (~100 mg·L^{-1}) for different time intervals (0.5 – 6 h).

pH-dependent experiments were carried out by adjusting the initial pH (in the range 5 – 12) using 0.1 M HNO_3 or 0.1 M NaOH solutions. One hundred milligrams of K_{sd}3P10-LDH and K_{liq}3P10-LDH were weighed into polyethylene tubes and 20 mL of the stock solution were added and stirred for 4 h. Then, the mixture was centrifuged and supernatant fluoride concentration was determined.

The adsorption isotherms were obtained by the batch equilibrium technique. One hundred milligrams of K_{sd}3P10-LDH and K_{liq}3P10-LDH were weighed into polyethylene tubes and then these were filled with 20 ml of aqueous solutions of NaF (the pH of mixture was adjusted at pH~6) ranging in concentration from 0 to 1000 mg F/L^{-1}. The mixtures were stirred for 4 h in room temperature, centrifuged and the supernatant fluoride concentrations were determined.

3. Results and discussion

3.1. Characterization of the clay. The sample selected for this study is Tabarka clay (Tunisian clay).

XRD: the nature of the impurities was determined by examining the crude sample. Quartz (reflection at 3.35 Å) is the major impurity. The diffractogramme of purified sample (Fig.1, *a*) shows the reflections at *d* = 7.21 Å and 10.05 Å characteristic of the kaolinite and illite respectively [24].

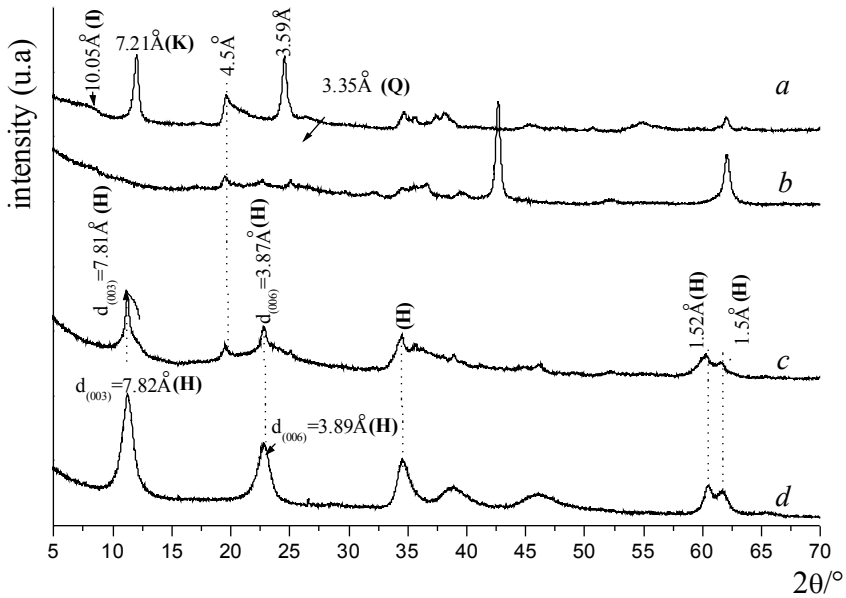

Fig. 1. X-ray patterns of clay sample: (a) purified clay; (b) Clay + $Mg(NO_3).6H_2O$ and heated at 500°C; (c) K_{sd}3P10-T150; (d) K_{liq}3P10.[(K) Kaolinite, (I) Illite, (Q)Quartz,(H) hydrotalcite

Fig.1, *b* shows the powder XRD pattern of the mixture of kaolinitic clay and the magnesium nitrate after heating at 500°C. Due to the absence of the peak corresponding of the *d*-spacing of 7.21 Å and attributed of the kaolin in the XRD pattern of the product shows that the structure of the original clay is completely destroyed and indicates the metal oxide peaks, suggesting an almost total decomposition of the original clay. This observation is consistent with the result given by the study of the thermal stability for the clay sample.

***Infrared spectra*:** Fig. 2, *a* shows the Infrared spectra of purified clay over the wavenumber range of 4000 – 400 cm^{-1}. The figure shows that purified sample contains quartz (800 cm^{-1}). The spectrum exhibited the characteristic band at 3697 cm^{-1} confirming the dominant presence of kaolinite. The band, at 1637 and 3450 cm^{-1} corresponds to the bonding modes of absorbed water.

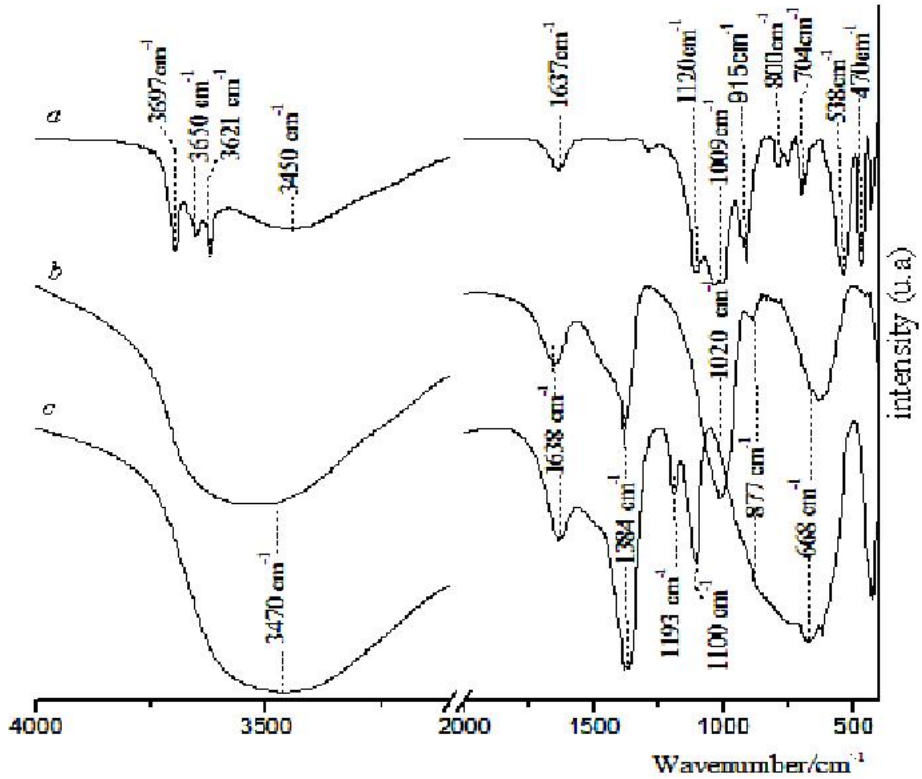

Fig. 2. Infrared spectra of: (a) purified clay; (b) K_{sd}3P10-T150; (c) K_{liq}3P10

3.2. Characterization of the adsorbent K_{liq}3P10-LDH and K_{sd}3P10-LDH. *Powder XRD.* Fig.1, *c* and Fig.1, *d* show the XRD patterns for the precipitates obtained by method 1 and method 2 respectively. It is shown that the K_{sd}3P10-LDH and K_{liq}3P10-LDH samples patterns were comparable to

that pattern of the sample prepared by the conventional method. The K_{liq}3P10-LDH sample showed a layered structure as observed from the peaks at 7.82, 3.89 and 2.61 Å, corresponding to planes (003), (006) and (009) for a layered hydrotalcite-like material, respectively [25]. The K_{sd}3P10-LDH sample display very weak and broad peaks at a 2Θ value of 11° compared to the sample prepared by coprecipitation at the same conditions (pH = 10 and $Mg^{2+}/Al^{3+} = 3$). K_{sd}3P10-LDH shows a structure different from the previous samples; it was an ill-defined hydrotalcite contaminated with argillaceous phase ($d = 4.5$ Å).

IR spectroscopy. The FT-IR spectra of the K_{sd}3P10-LDH and K_{liq}3P10-LDH were presented in Fig. 2, *b* and Fig. 2, *c*. It shows a broad band around 3470 cm^{-1} due to the stretching mode of the structural – OH groups in the metal hydroxide. However, a small shoulder at 2900 – 3000 cm^{-1} suggests the presence of a second type of – OH stretching vibration (possibly due to hydrogen bonding with carbonate in the interlayer spacing [26].

The two spectra show: (i) A shoulder at 1638 cm^{-1} is ascribed to the bending mode of the interlayer water molecules [27].

(ii) The three characteristic bands of carbonate in hydrotalcite at around 1384 cm^{-1} ($н_3$), 877 cm^{-1} ($н_2$) and ~1020 cm^{-1} ($н_1$) [28 – 29].

(iii) The bands around 420 and 668 cm^{-1}, which are ascribed to the bending mode Al – O and Mg–O.

The infrared spectrum of the K_{liq}3P10-LDH shows additional bands appearing at 1193 and 1100 cm^{-1} which could not be identified.

Surface area and N_2 adsorption-desorption studies. The N_2 adsorption-desorption isotherm is of type II for all samples, which is typical of mesoporous materials (Fig. 3). All of the materials possessed zero micropore volume. Adsorption isotherms of this type are represented by mesoporous materials with no micropores and strong interactions between adsorbent and adsorbate molecules. This type of hysteresis loop is formed when the adsorption and desorption curves do not coincide and is caused physically by the phenomenon of capillary condensation in the mesopores.

From Fig. 3, it was determined that all samples show a horizontal course of the hysteresis branch over an appreciable range of gas uptake ($P/P_0 = 0.6$), while it is vertical above this ratio. This type of hysteresis loop is often observed with aggregates of plate-like particles that give rise to slit-shaped pores.

Specific surface areas of the K_{sd}3P10-(500)-LDH and K_{liq}3P10-(500)-LDH were determined by the single-point BET method (Table 1) and were found to be 179 and 165 m^2g^{-1} respectively, much greater than the 80 and 78 m^2g^{-1} values obtained for their precursors at the precursor temperature at 150°C. It was suggested that a porous system was developed in the calcined sample during the transformation of CO_3^{2-} to CO_2 [30].

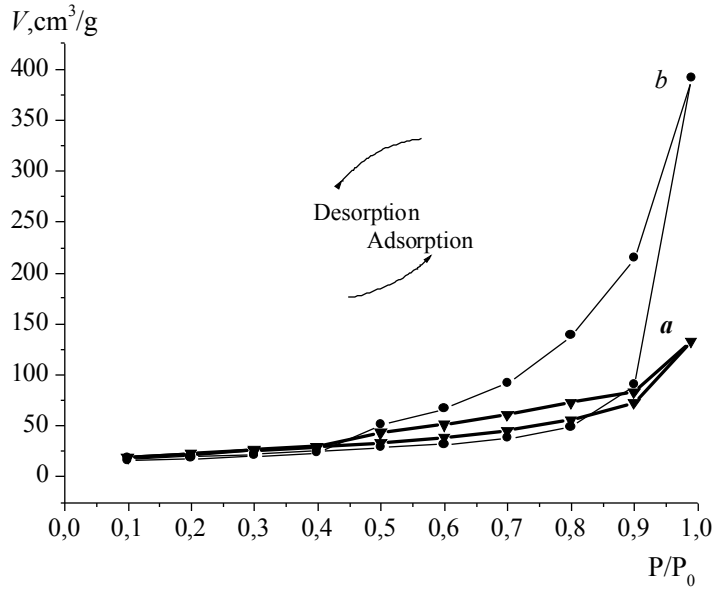

Fig. 3. N_2 adsorption-desorption isotherms: (a) K_{sd}3P10-LDH; (b) K_{liq}3P10-LDH

Table 1. Textural properties for various sorbent samples

	K_{sd}P10		K_{liq}P10	
	S_{BET}, m^2/g	$V_{macropore}$, cm^3/g	S_{BET}, m^2/g	$V_{macropore}$, cm^3/g
Before alcination	80	0.2044	78	0.6052
After calcination	178	–	165	–

PZC determination. Batch equilibrium method for determination of the point of zero charge (PZC) was proposed by [31]. Accordingly, the samples of calcined hydrotalcite (0.1g) were shaken in PVC vials, for 24 h, with 30 ml of 0.01M KCl, at different pH values. Initial pH values were obtained by adding a certain amount of KOH or HCl solution so that to keep the ionic strength constant. Experimental results of the pH_{pzc} determination are given in Fig. 4. They are presented as pH values of filtered solutions equilibration (pH_f) with calcined HT as a function of initial pH value (pH_i). It can be seen that PZC is at pH = 8.6 and 8.5 (pH_f level, where common plateau is obtained) for K_{sd}3P10-(500)-LDH and K_{liq}3P10-(500)-LDH respectively.

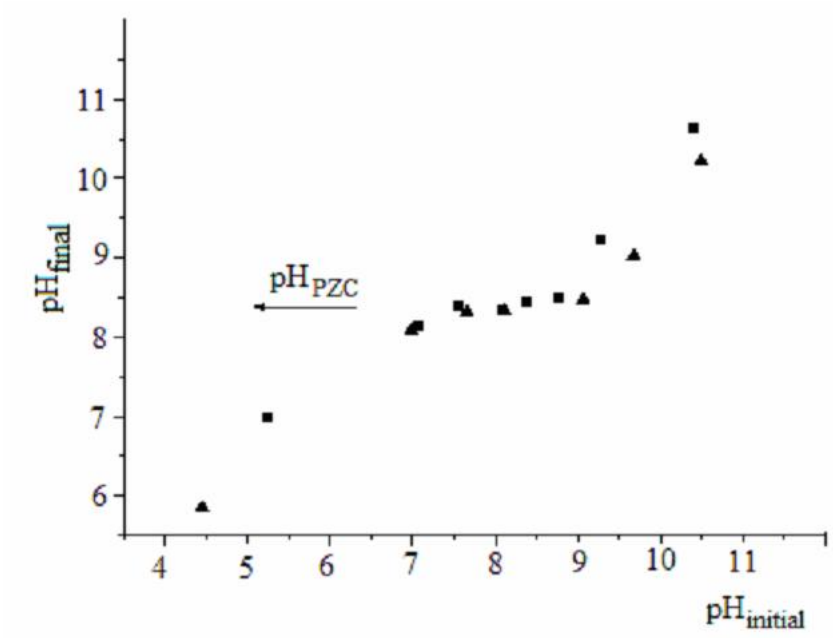

Fig. 4. Determination of pH_{PZC} of (n) K_{sd}3P10-(500)-LDH and (%) K_{liq}3P10-(500)-LDH in KCl solution

3.3. The optimisation of the operating conditions of adsorption

3.3.1. The effect of pH. Generally, the pH is an important variable; it controls the adsorption at water-adsorbent interfaces. Therefore, the adsorption of fluoride on the CLDH was examined at different pH values ranging from 5.0 to 10.0 and relevant data are presented in Fig. 5.

Fig. 5 shows that the adsorption value increases with the increase in pH and reaches maximum (70% and 80% for K_{sd}3P10-(500)-LDH and K_{liq}3P10-(500)-LDH, respectively) at the pH of 6.3 before decreasing to ≈ 40% at pH 12.5. However, at low pH (pH < 6), the adsorption capacity was low, probably due to the protonation of the F ions and dissolution of the layered materials in acid medium, this observation has been confirmed by the analysis of Mg, which presents in the resulting solution after the adsorption assisted by atomic absorption spectrometry. Therefore, an optimal pH value should be near that of 6.0. This is important inference, since the pH values of most water streams vary from neutral to weakly basic range except for the acid drainages. Similar observations have been made on the pH dependence of fluoride adsorption with ZnAl-Cl-LDH, in which the fluoride uptake decreased with the increasing pH [32].

As the pH approached that corresponding to the PZC of calcined LDH, the surface charge decreased resulting in reduced F LDH interactions leading to low F uptake. An increase in the concentration of the competing OH anions at pH above 7 might also be responsible for the observed decrease in the

adsorption capacity at higher pH. Similar changes of the adsorption capacity with solution pH have been reported by Das et al. [33].

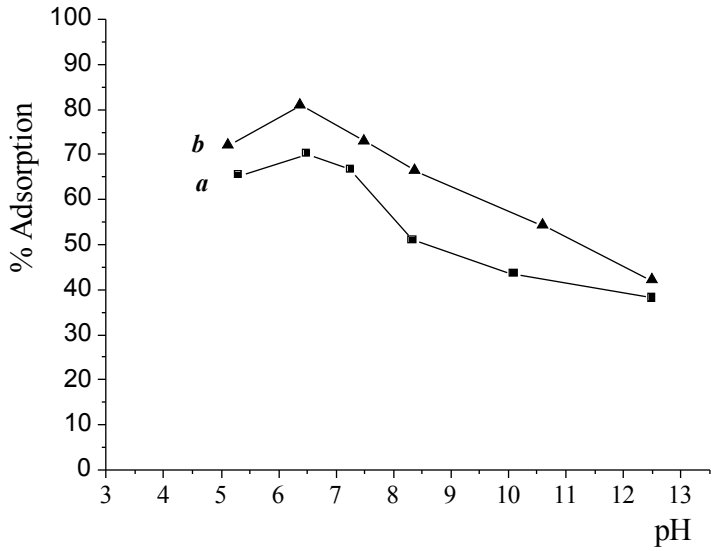

Fig. 5. The percentage of fluoride removal by (a) K_{sd}P10-(500) and (b) K_{liq}P10-(500) as a function of pH variation

3.3.2. Effect of contact time. The variation of fluoride adsorption as a function of time is shown in Fig. 6. The kinetic curves show that the equilibrium time and adsorption capacity of K_{sd}P10-(500) and K_{liq}P10-(500) are similar. We observed that adsorption of fluoride is a fast process on HT-like compounds. This behaviour has already been reported in the adsorption of anionic species on HT-like compounds [34].

For K_{liq}3P10-(500)-LDH used as a sorbent, the plot of the removed amount of fluoride gives an initial steep portion (~30 mn) followed by the slow increase for approximately 1h. The yield of fluoride removal was of 65%. For K_{sd}3P10-(500)-LDH, the period of 3 h was necessary for reaching equilibrium and the maximum percentage of fluoride removal was of 65%. It is well known that HT- like compounds interacts strongly with anionic species due to the existence of positive charges on the lamellae and also over their external surface [35]. This property makes possible the occurrence of two different mechanisms of anion removal: (i) adsorption on external surface (fast process) and (ii) anion exchange (slow process) [16].

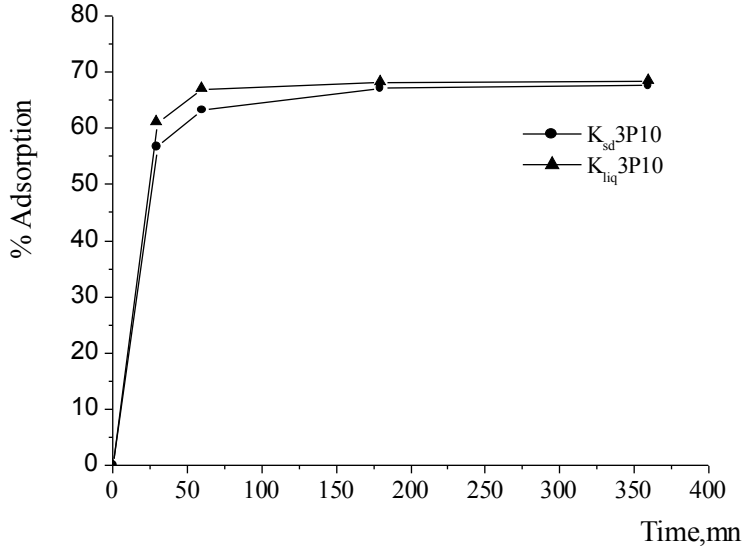

Fig. 6. Effect of time on fluoride adsorption on (%) K_{sd}3P10-(500)-LDH and (%) K_{liq}3P10-(500)-LDH (C_0= 600 mgF·L^{-1} and pH 6)

The adsorption process depends on the variable charge density on the surface as well as on the surface area of the adsorbent. The ion exchange depends on the nature of the interlayer anions represented in the sample [36, 37]. Generally, the adsorption process is faster than the anion exchange because of the strong interaction between negative ions and the positive external surface and due to the high exposition of the external surface of LDH, while ion exchange is a diffusion process. Moreover, in this study, the fluoride removal is realized by sorption process followed by a rebuilding of the initial structure with fluoride anion in the interlayer space.

Generally, three steps are involved in the process of sorption by porous particles [19] (i) external mass transfer (by mechanism of boundary layer or film diffusion) between the external surface of the sorbent particles and surrounding fluid phase; (ii) inner transport within the particle; and (iii) chemisorption (reaction kinetics at phase boundaries), where the rate of adsorption is generally controlled by the kinetics of bond formation.

Kinetic modeling not only allows estimation of sorption rates but also leads to suitable rate expressions characteristic possible reaction mechanisms. In this respect, several kinetic models including the pseudo-first-order (Eq.(1)), pseudo-second-order equation (Eq.(2)) and intraparticle diffusion model (Eq.(3)) [38] were tested.

$$\frac{1}{Q_t} = \left(\frac{k_1}{Q_m}\right)\left(\frac{1}{t}\right) + \frac{1}{Q_m}, \quad (1)$$

$$\frac{t}{Q_t} = \frac{1}{k_2 Q_m^2} + \frac{t}{Q_m}, \quad (2)$$

$$Q_t = k_p t^{1/2} + C, \quad (3)$$

here is the amount of fluoride sorbed (mg/g) at a given time, the maximum adsorption capacity (mg/g), and the pseudo-first-order and pseudo-second-order rate constant, respectively, the intraparticle diffusion rate constant and C is the intercept. The calculated kinetic parameters for fluoride sorption by calcined K_{sd}P10 and K_{liq}P10 are given in table 2.

Table 2. Kinetic parameters for sorption of fluoride by K_{sd}P10-(500) and K_{liq}P10-(500)

	k_1 (h^{-1})	Q_1 (mg/g)	R_1^2	k_2 (g/mg h)	Q_2 (mg/g)	R_2^2	k_p (g/mg h)	C (mg/g)	R_p^2
K_{sd}P10-(500)	0.111	92.59	0.99	0.118	91.74	1.0	7.55	73.71	0.76
K_{liq}P10-(500)	0.065	93.45	0.91	0.023	91.74	1.0	4.55	81.492	0.58

It seems that, of the three kinetic equations tested, the pseudo-second-order best described the kinetic data for fluoride sorption by calcined LDH (Fig. 7), based on the correction coefficient R^2. The pseudo-second-order equation is based on the adsorption loading of the solid phase and is in agreement with a chemisorption being the rate determining step mechanism.

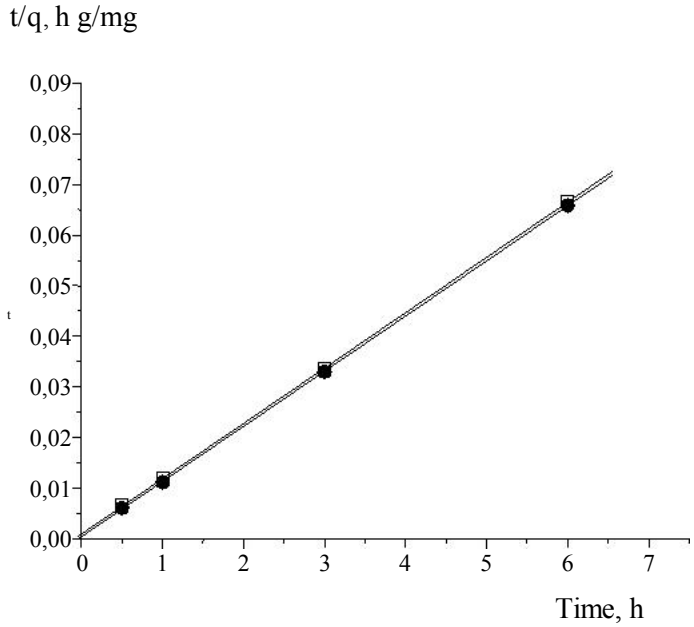

Fig. 7. Pseudo-second-order kinetics model. Plot of (t/q_t) as a function for time (□) *K_{sd}P10-(500)-LDH (R^2 = 1.0) and (●) K_{liq}P10-(500)-LDH (R^2 =1.0)*

3.3.3. Effect of the adsorbent dosage. The fraction of fluoride removal increases with the increase of the adsorbent dose from 0.5 to 4.0 g/L at a fixed fluoride concentration (600 mg F/L), pH 6 and temperature of 303 K (Fig. 8). This is consistent with the argument that surface sites of oxide systems are heterogeneous [39, 40]. According to this model; there is a spectrum of binding energies of the adsorption sites. At a low fraction of adsorbent, all types of sites are fully exposed to the interaction with the adsorbate, and the surface saturation is reached rapidly. For higher particle concentrations, the availability of sites with high energy decreases, while a larger fraction of low energy sites are occupied. That is, the number of active adsorption sites is larger at a fixed adsorbate concentration. The given plot shows a maximum of fluoride removal at an adsorbent concentration of 3 g/L, while Liang et al. 2006 [41] were found that 1.1 g/L is sufficient to have a maximum of fluoride removal using Mg – Al – CO_3– LDH synthesized by conventional method.

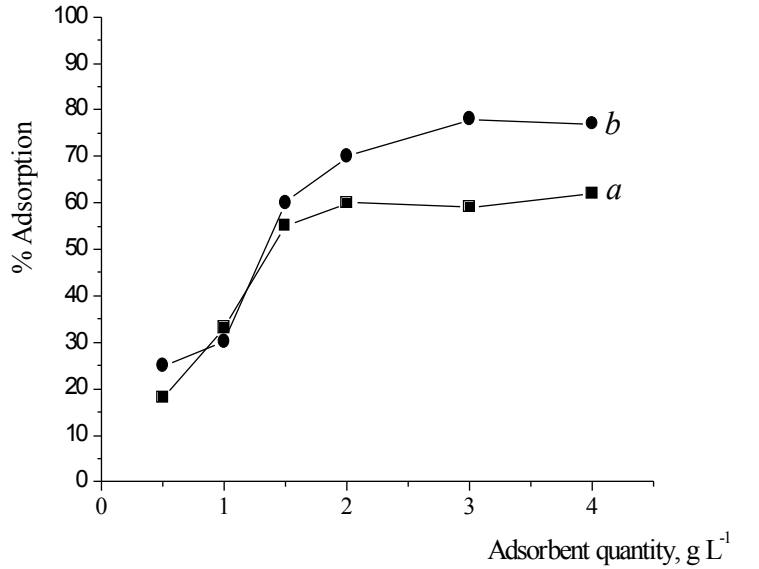

Fig. 8. Effect of adsorbent dose on the fluoride removal at adsorbate concentration 600 mg/L, pH ~ 6.3, and temperature 303 K: (a) K_{sd}P10-500-LDH and (b) K_{liq}P10-(500)-LDH

3.3.4. Effect of ionic strength. The effect of ionic strength on fluoride anion adsorption was studied by conducting batch experiments at varied ionic strength of 0.001, 0.01 and 0.1 M KCl. The results are shown in Fig. 9. The fluoride uptake varies depending on the salinity solution due to the presence of competing anions. The percentage of fluoride uptake decreases steeply from 60 to 38 for K_{sd}P10-(500)-LDH and 80 to 50 for K_{liq}P10-(500)-LDH with an increase in the ionic strength from 0.001 to 0.01 M and decreases slowly to 35 and 45, for K_{sd}P10-(500)-LDH and for K_{liq}P10-(500)-LDH, respectively, for an ionic strength of 0.1 M KCl. The influence of ionic strength is more pronounced in the region of low values. This suggests the presence of two types of adsorption sites in the samples; (*a*) non-specific sites only capable of weak interactions, and (*b*) specific ones that strongly interact with fluoride ions. The non-specific sites may be sensitive to the coexisting anions, and therefore the adsorbed fluoride may be easily exchanged with Cl^- ions from solution even at low concentration. The fluoride ions adsorbed on the strong specific sites are rarely substituted on the surface even in a solution with a large excessive amount of coexisting ions. However, we cannot distinguish the strong specific sites and weak non-specific ones due to the nearly amorphous structure of the samples. Similar observations have been made on the ionic strength dependence of fluoride adsorption with calcined Mg – Al – CO_3–LDH in aqueous solution, in which the fluoride uptake decreased where Cl^- exists in solution [41].

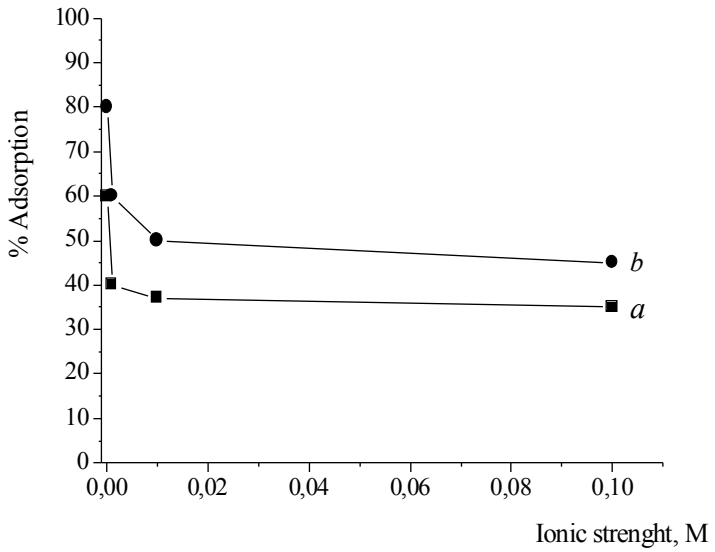

Fig. 9. Effect of ionic strength on the sorption of fluoride by (a) K_{sd}P10-(500)-LDH and (b) K_{liq}P10-(500)-LDH (C_0=600 mg/L and pH 6)

3.4. Adsorption isotherms. Equilibrium adsorption isotherms are of fundamental importance in the study of adsorption systems since they indicate how the anionic species partition themselves between the medium and liquid phase with increasing concentration at equilibrium. When medium and anionic species solutions are contacted, the concentration of the anions on the medium will increase until a dynamic equilibrium is reached, at which point there is a defined distribution of anionic species between the solid and liquid phases. The adsorption isotherms were constructed using the batch equilibrium technique where a fixed mass of adsorbent (100 mg) was agitated with fluoride solution of various concentrations (0–800 mg/L) for a sufficient length of time to ensure equilibrium had been achieved. An agitation time of 4h and equilibrium temperature of 25°C were used.

Sorption isotherms of fluoride retention by calcined LDH are shown in Fig. 10. It is evident that sorption capacity of K_{liq}P10-(500) is much larger than these of K_{sd}P10-(500)-LDH. For example, at a similar fluoride concentration of 100 mg/L sorption capacity of K_{liq}P10-(500) was greater three times than that of K_{sd}P10-(500)-LDH. These results can be explained by the fact that K_{sd}P10-(500)-LDH contains an argillaceous phase as impurity. Indeed, the PZC of silica, which coming from the argillaceous phase, is ~ 2 thus at pH 6, the surface of silica is charged negatively what disadvantages the adsorption of the ions fluoride.

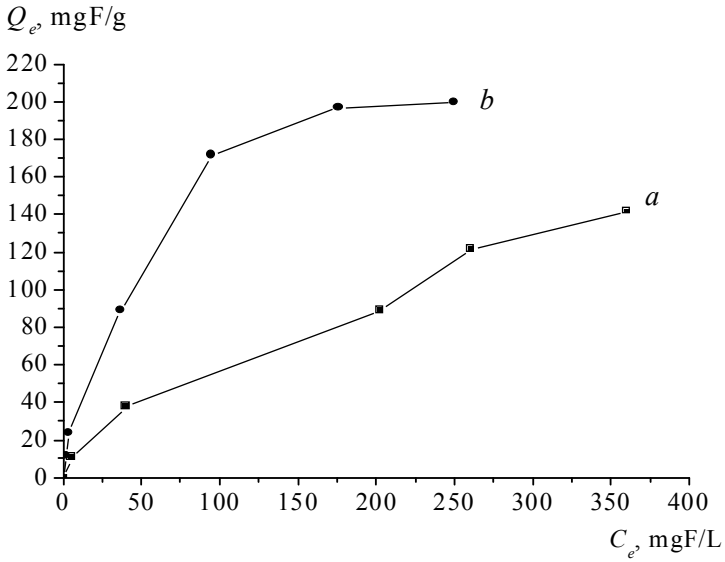

Fig. 10. Equilibrium isotherms of fluoride removal on (a) K_{sd}P10-(500)-LDH and (b) K_{liq}P10-(500)-LDH

Isotherms for fluoride sorption by K_{sd}P10-(500)-LDH and K_{liq}P10-(500)-LDH were modeled by two commonly used isotherm equations, Langmuir (Eq. 4) [42] and Freundlich (Eq. 5) [43].

$$Q_e = K_F C_n^e \quad (4)$$

or

$$\log Q_e = \log K_F + n \log C_e \quad (5)$$

where Q_e (mg/g) is the amount of fluoride sorbed at equilibrium, Q_m (mg/g) the theoretical maximum monolayer sorption capacity, C_e (mg/L) the equilibrium concentration of fluoride in solution, and K_F, n and K_L are empirical constants. The calculated Langmuir and Freundlich isotherm constants are given in Table 3. Data for fluoride sorption by K_{sd}P10-(500)-LDH and K_{liq}P10-(500)-LDH were fitted better by Freundlich equation than by the Langmuir equation based on the correction coefficient R^2. The best fit Freundlich parameters are K_F = 4.21 and 10.26, n = 0.5936 and 0.5962 for K_{sd}P10-(500)-LDH and K_{liq}P10-(500)-LDH respectively. The n value in the range of 0.1–1 indicates a favorable adsorption process. The best fit Langmuir parameters are Q= 175 and 213.22 mg/g, K_L = 0.008 and 0.017 L/mg for K_{sd}P10-(500)-LDH and K_{liq}P10-(500)-LDH respectively.

The removal of fluoride by different adsorbents has been studied in recent years and some of these reports provide Q values. Although these values were

obtained under different ranges of conditions, they can be useful in criterion of the adsorbent capacity. The Q value obtained in this study is greater than those of reported for alum sludge (5.394 mg/g) [44], actived alumina (16.34 mg/g) [45], flyash (20 mg/g) [13], lignite (7.09 mg/g) and bituminous coal (7.44 mg/g) [46].

Table 3. Langmuir and Freundlich isotherm constant for sorption of fluoride by K_{sd}P10-(500) and K_{Liq}P10-(500)-LDH

	Langmuir			Freundlich		
	Q_m (mg/g)	K_L (L/mg)	R^2	n	K_F (L/g)	R^2
K_{sd}P10-(500)	175	0.008	0.9023	0.5936	4.21	0.9968
K_{Liq}P10-500)	238	0.017	0.9705	0.5962	10.26	0.9826

R^2: Correction coefficient.

The mechanism of removal of fluoride ions by calcined LDH can be explained as follows.

The regeneration of LDH is due to the ability of calcined LDH to incorporate anions into its structure by means of the so-called "memory effect". LDH containing carbonates as the interlayer anion decomposes into magnesium and aluminum oxides when heated at 500°C. The calcined product $Mg_{1-x}Al_xO_{1+x/2}$ can be rehydrated and incorporate anions, such as fluoride, to rebuild the initial layered structure.

$$[Mg_{1-x}Al_x(OH)_2](CO_3)_{x/2} \rightarrow Mg_{1-x}Al_xO_{1+x/2} + (x/2)CO_2 + H_2O\ ; \quad (6)$$

$$Mg_{1-x}Al_xO_{1+x/2} + (x)F^- + (1 + (x/2)+y)H_2O \rightarrow [Mg_{1-x}Al_x(OH)_2](F)_x + xOH^-. \quad (7)$$

OH^- is produced during rehydration of CLDH. As a result, controlling the pH of solution is important in order to maintain a driving force for removal of fluoride ion by CLDH [42].

Structural reconstruction was confirmed by XRD analysis. The XRD pattern of K_{sd}P10-(500) (Fig. 11, *a*) and K_{liq}P10-(500) (Fig.12, *a*) are evidence of the presence of mixed oxide phase, which possesses a typical poorly crystalline MgO-like structure.

Upon addition of the thermally activated hydrotalcite to an aqueous solution containing sodium fluoride the so-called "memory" effect or reformation effect of hydrotalcites comes into play. Hydrotalcites after thermal decomposition will regain their original structure, providing the compound is not heated to

too high a temperature. The XRD pattern of the fluoride adsorbed HT shows a d_{003} spacing of 7.63 and 7.65 E for K_{sd}P10-(500) and K_{liq}P10-(500)-LDH respectively. These basal spacing values are weaker than of the original samples, what indicates that fluoride ions are intercalated in the interlayer space, because F has a radius smaller than carbonate ion.

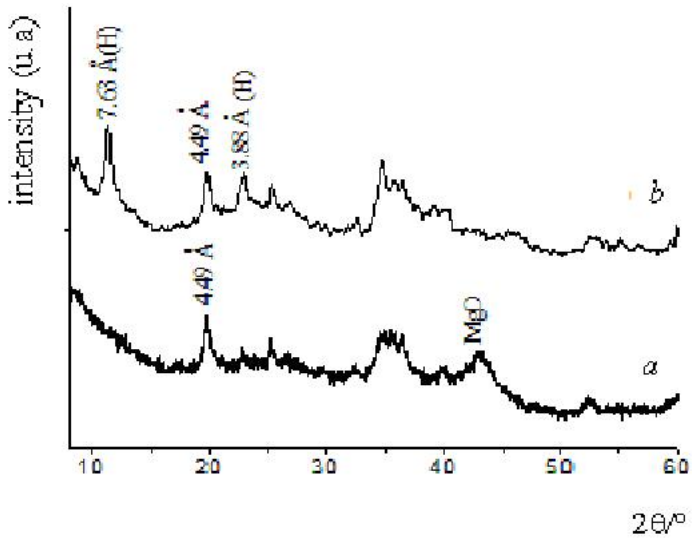

Fig. 11. XRD powder spectra of the: (a) K_{sd}P10-(500) and (b) K_{sd}P10-(500) after a contact with the fluoride solution

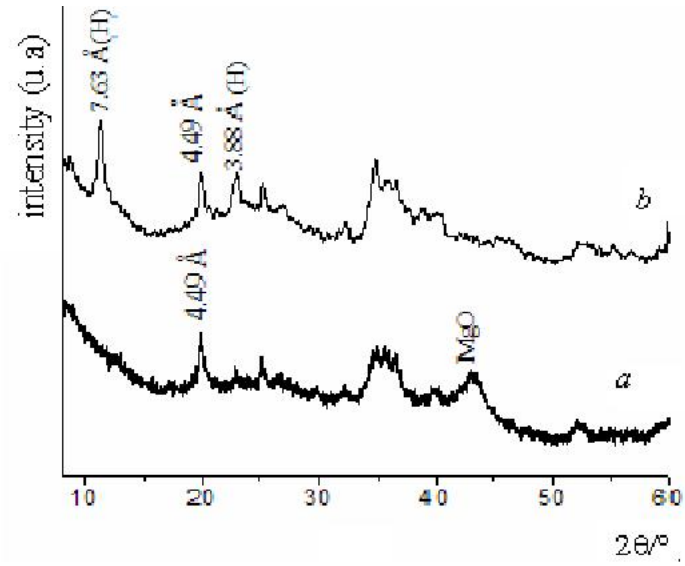

Fig. 12. XRD powder spectra of the: (a) K_{liq}P10-(500) and (b) K_{liq}P10-(500) after a contact with the fluoride solution

The XRD pattern in Fig.12, *b* which corresponds to the product obtained after the interaction of K_{liq}P10-(500)-LDH with F^- reveals additional reflections other than of the hydrotalcite structure. These reflections were attributed to the formation of the aluminium fluoride phase which was formed by precipitation. What explains why Q_m (238 mgF^-/g) obtained by K_{liq}P10-(500)-LDH is large compared to that is obtained by K_{sd}P10-(500) (Q_m=175 mg/g). The calcined LDH after removal of fluoride can be regenerated using Na_2CO_3 aqueous solution (0.1 mol/L) followed by calcination at 500°C. It can be concluded from the above observations that the adsorption of fluoride is a reversible process, thereby facilitating the recyclability of the material for further use.

4. Conclusion

This work describes a new method to remove fluoride from aqueous solutions that is promising for the treatment of wastewater in industrial processes. The fluoride removal from water by calcined HT synthesized by co-precipitation (K_{liq}P10-(500)-LDH) and by mechanochemical synthesis method (K_{sd}P10-(500)-LDH) using the kaolinitic clay as trivalent cation resource.

Our results show that the calcined LDH synthesized from the cationic clay has a marked ability to adsorb fluoride. The adsorption loading is higher for K_{liq}P10-(500)-LDH than that of K_{sd}P10-(500)-LDH. It was found that fluoride sorption occurs with a high extraction rate and the removal of fluoride by calcined HT strongly depends on the process parameters. The increase of pH from 5 to 13 results in a reduction of the positive charge of the adsorbent that leads to a decrease of the amount of adsorbed fluoride. The maximum removal of fluoride from aqueous solutions occurs at pH 6.3 in 4 h and the retention of fluoride ions by the CLDH material was ~80% or higher. The increase in the ionic strength by the addition of KCl results in a large decrease in the amount of removed fluoride. This effect is probably due to the enhancement of anion exchange during the adsorption process. Equilibrium results could be fitted by the Freundlich isotherm and Langmuir isotherm, and the former is a better model. The Freundlich constant (n) in the range of 0.1–1 indicates a favorable adsorption process. The maximum adsorption capacity is 238 and 175 mg/g for K_{liq}P10-(500)-LDH and K_{sd}P10-(500)-LDH, respectively, higher than that reported on other adsorbents for fluoride removal. A mechanism of the adsorption phenomenon has been proposed on the basis of XRD. Overall, the results demonstrate the convenient synthesis of the hydrotalcite from the kaolinite and the high efficiency of fluoride removal that is promising for potential applications of calcined K_{liq}P10 and K_{sd}P10-LDH in the environmental clean-up and remediation of contaminated water.

Резюме. Исследована сорбция фторида на Mg–Al–CO_3, полученном из каолинита как природного источника алюминия с использованием двух простых методов. В первом методе применен каолинит в твердом состоянии; во втором – фильтрат каолинита после растворения подкисленными растворами. В лабораторных условиях оценены характеристики адсорбции фторида из синтетической сточной воды на кальцинированных образцах LDH. Исследовали анионные глины [K_{sd}3P10-T150] (синтезированная по первому методу) и [K_{liq}3P10] (синтезированная по второму методу). Равновесная изотерма показала, что извлечение фторид-иона соответствует уравнениям Ленгмюра и Фрейндлиха и модель Фрейндлиха лучше соответствует экспериментальным данным, чем модель Ленгмюра. Максимальная адсорбционная емкость составляет 238 и 175 мг/г соответственно для K_{liq}P10-(500)-LDH и K_{sd}P10-(500)-LDH, что выше, чем значения, приводившиеся для других адсорбентов, которые применялись для удаления фторида. Механизм удаления фторид-ионов подтвержден рентгеновской дифракцией. Результаты демонстрируют эффективный путь синтеза гидротальцита из каолинита и высокую степень удаления фторида, которая является многообещающей для применения кальцинированных глин K_{liq}P10 и K_{sd}P10-LDH в очистке объектов окружающей среды и загрязненных вод.

Резюме. Досліджена сорбція фториду на Mg–Al–CO_3, отриманому з каолініту як природного джерела алюмінію з використанням двох простих методів. У першому методі використовується каолініт в твердому стані; у другому – фільтрат каолініту після розчинення розчинами, що підкисляють. У лабораторних умовах оцінені характеристики адсорбції фториду з синтетичної стічної води на кальцинованих зразках LDH. Досліджували аніонні глини [K_{sd}3P10-T150] (синтезована першим методом) і [K_{liq}3P10] (синтезована другим методом). Рівноважна ізотерма показала, що витягання фториду-іона відповідає рівнянням Ленгмюра і Фрейндліха і модель Фрейндліха краще відповідає експериментальним даним, чим модель Ленгмюра. Максимальна адсорбційна ємність складає 238 і 175 мг/г відповідно для K_{liq}P10-(500)-LDH і K_{sd}P10-(500)-LDH, що вище, ніж значення, які приводилися для інших адсорбентів, що застосовувалися для видалення фториду. Механізм видалення фторид-іонів підтверджений рентгенівською дифракцією. Результати демонструють ефективний спосіб синтезу гидротальцита з каолініту і високу міру видалення фториду, яка є багатообіцяючою для вживання кальцинованих глин K_{liq}P10 і K_{sd}P10-LDH в очищенні об’єктів довкілля і забруднених вод.

1. *Chinoy N.J., Narayana M.V.*// Reprod. Toxicol. – 1994. – **8**. – P.155.
2. *World* Health Organization. – 1984. – **2.** – P. 249.
3. *Reardon E.I., Wang Y.* // Environ. Sci. and Technol. – 2000. – **34**. – P. 3247.
4. *Wasay S.A., Haron M.J. Tokunaga S.* //Water Environ. Res. – 1996. – **68**. – P.295.
5. *Raichur A.M., Basu M.J.* //Sep. Purif. Technol. – 2001. – **24**. – P.121.
6. *Lounici H., Belhocine D., Grib H., Drouiche M., Pauss A., Mameri N.* //Desalination. – 2004. – **161. –** P.287.
7. *Mohapatra D., Mishra D., S.P.Mishra, G.R. Choudhury, R.P. Das* //J. Colloid and Interface Sci. – 2004. – **275**. – P.355.
8. *Ghorai S., Pant K.K.* // Sep. Purif. Technol. – 2005. – **42**. – P. 265.
9. *Onyango M.S., Kojima Y., Aoyi O., Bernardo E.C., Matsuda H.* //J. Colloid and Interface Sci. – 2004. – **279**. – P.341
10. *Agarwal M., Rai K., Shrivastav R., Dass S.* //J. Clean. Prod. – 2003. – **11**. – P.439.
11. *Ramos R.L., Ovalle-Turrubiartes J., Sanchez-Castillo M.A.* //Carbon. – 1999. – **37**. – P.609.
12. *Li Y.H., Wang S., Zhang X., Wei J., Xu C., Luan Z., Wu D.*// Mater. Res. Bull. – 2003. – **38**. – P.469.
13. *Chaturvedi A.K., Yadav K.P., Pathak K.C., Singh V.N.*// Water Air Soil Pollut. – 1990. – **49**. – P.51.
14. *Cengeloglu Y., Kir E., Ersoz M.*// Sep. Purif. Technol. – 2002. – **28**. – P.81.
15. *Bulusu K.R., Sundaresan B.B., Pathak B.N., Nawlakhe W.G., Kulkarni D.N. Thergaonkar V.P.*// J. Inst. Eng. Environ. Eng. – 1979. – Div 60.
16. *Cavani F., Trifiro F., Vaccari A.*// Catal. Today. – 1991. – **11**. – P.173.
17. *Orthman J., Hu H.Y., Lu G.Q.*// Sep. Purif. Technol. – 2003. – **31.** – P.53.
18. *Goswamee R.L., Sengupta P., Bhattacharyya K.G., Dutta D.K.*// Appl. Clay Sci. – 1998. – **13**. – P. 21.
19. *Lazaridis N.K., Asouhidou D.D.*// Water Res. – 2003. – **37**. – P.2875.
20. *Toraishi T., Nagasaki S., Tanaka S.*// Appl. Clay Sci. – 2002. – **22**. – P.17.
21. *Das D.P., Das J., Parida K. J.* //J.Colloid and Interface Sci. – 2003. – **261**. – P.213.
22. *Ren Z.F., He J., Zhang C., Duan X.*// Fine Chem. – 2002. –**19**. – P.339.
23. *Diaz-Nava C., Solache-Rios M., Olguin M.T.*// Sep. Sci. Technol. – 2003. – **38**. – P.131.
24. *Brindley G., Brown G.* Mineralogical Society. – London, 1984. – P.64.
25. *De Roy A., Forano C., El Malki K., Besse J-P.*// Synthesis of microporous materials.– New-York: Van Nostrand Reinhold, 1992. – P. 108 –169
26. *Das J., Das D., Parida K.M.*// J. Colloid. and Interface. Sci. – 2006. – **301**. – P.569
27. *Allegra G., Ronca G.*// Acta Crystallogr., A. – 1978. – 34. – P.1006.
28. *Alvarez-Ayuso E., Nugteren H.W.*// Water Res. – 2005. – **39**. – P.2535.
29. *Kloprogge J.T., Wharton D., Hickey L., Frost R.L.* // J. Amer. Mineralogist. – 2002. – **87**. – P. 623.

30. *Hermosin M.C., Pavlovic I., Ulbibarri M.A., Cornejo J.* // Water Res. – 1996. – **30**. – P.171.
31. *Milongic SK., Antonucci V., Minutoli M., Giordano N.*// Carbon. – 1975. – **27**.– P. 337
32. *Mandal S., Mayadevi S.* // Appl. Clay Sci. – 2008. – **40**. – P. 54.
33. *Das D.P., Das J., Parida K.*// J. Colloid and Interface Sci. – 2003. – **261**. – P.213.
34. *Frost R.L., Weier M.L., Martens W.N., Henryb D.A., Mills S.J.* // Spectrochim. Acta., A. – 2005. – **62**. – P. 181.
35 *Inacio J., Taviot Gueho C., Forano C., Besse J.P.* // Appl. Clay. Sci. – 2001. – **18.** – P. 255.
36. *Miyata S.*// Clays Clay Miner. – 1983. – **31**. – P.305
37. *Sato T., Wakabayashi T., Shimada M.*// J. Ind. Eng. Chem. Prod. Res. – 1986. – **25**. – P.89.
38. *Ozcan A.S., Ozcan A.*// J. Colloid and Interface Sci. – 2004. – **276.** – P.39.
39. *Catts J.G., Langmuir D.*// J. Appl. Geochem. – 1986. – **1**. – P.255.
40. *Honeyman B.D., Santschi P.H.*// J. Environ. Sci. and Technol. – 1988. – **22**. – P.862.
41. *Liang Lv., Jing He., Wei Min, Evans D.G., Duan Xue.* // J. Hazard. Materials, B. – 2006. – **133**. – P.119.
42. *Shin H.-S., Kim M-J., Nam S.Y., Moon H.C.* // Water. Sci. and Technol. – 1996. – **34.** – P. 161.
43. *Li Y.-H., Wang S., Zhang X.* // Mater. Res. Bull. – 2003. – **38.** – P. 469.
44. *Sujana M.G., Thakur R.S., Rao S.B.* // J. Colloid and Interface Sci. – 1998. – **206.** – P.94.
45. *Howard A., George K., Lindsay F.K.* // Ind. Eng. Chem. – 1938. – **30**. – P.163.
46. *Sivasamy A., Singh K.P., Mohan D., Maruthamuthu M.* // J. Chem. Technol. and Biotechnol. – 2001. – **76**. – P.717.

Centre National des Recherches en Sciences
des Materiaux (CNRSM),
Pole Technologique de Borj Cedria, Tunisia Recieved 17.09.2010